

Generation of cylindrically symmetric magnetic fields with permanent magnets and μ -metal

L. Ricci, C. Zimmermann, V. Vuletić, T. W. Hänsch

Max-Planck-Institut für Quantenoptik, D-85748 Garching, Germany
and Sektion Physik, Universität München, D-80799 Munich, Germany
(Fax: +49-89/285192)

Received 28 April 1994/Accepted 11 May 1994

Abstract. A method that allows the calculation of magnetic fields produced by cylindrically symmetric configurations of permanent magnets and high permeability materials is presented. The method is based on a non-iterative finite-element algorithm and can be utilized on small-scale computing facilities. As an example, the design of a magnetic trap for neutral atoms is discussed. Comparisons of calculations with analytical and experimental data are also reported.

PACS: 02.70.Dh, 07.55.+x, 85.70.Nk

The careful design of homogeneous and inhomogeneous magnetic fields is of critical importance to many applications in physics. The traditional sources of these fields are conventional or superconducting currents. Though these systems are well understood, reliable, and quite convenient for many applications, they can also be cumbersome, complicated, and expensive. Recently, the use of Rare-Earth permanent Materials (REMs) has emerged as a suitable alternative to traditional sources, not only duplicating the features of the older techniques, but in some cases achieving better results [1]. In particular, if the experimental requirements include a large magnetic gradient, then the combination of high permeability materials with REMs can yield a gradient substantially larger than possible with traditional sources. However, the resulting fields and gradients are notoriously difficult to calculate for such a combined system. In this paper, we present a technique which substantially simplifies the calculation for cylindrically symmetric configurations. We also present experimental confirmation of the technique's accuracy.

Though the remanence of REMs is comparable with that of traditional magnets (e.g., Alnico), they have an almost linear demagnetization curve and a much higher coercivity. Therefore, a relatively small REM can store a remarkably high magnetic energy density and produce a considerable amount of magnetic field flux, while maintaining the operation point sufficiently far away from the

“knee” of the demagnetization curve. Two of the more common REMs are samarium-cobalt and neodymium-iron-boron. These magnetic materials are already employed to generate magnetic multipoles with both translational symmetry and high intensity for nuclear magnetic resonance applications [2], twistors, wigglers and undulators in free-electron lasers [3], and accelerators. The design of magnetic multipoles with translational symmetry is extensively treated in the literature [4, 5]. Potential applications of REMs are the construction of magnetic dipoles with high field uniformity for Penning traps [6], mass spectroscopy, and the purely magnetic confinement of paramagnetic neutral atoms [7–9]. For this last goal, with the exception of the dipole field, magnetic spherical multipole fields with cylindrical symmetry are suitable. The magnetic potential for a given $2n$ -pole field is described by the n -th Legendre polynomial $r^n P_n(\cos \theta)$. A detailed description of the analytical design of such fields by using cylindrical magnets only is given in [10]. The design can even be optimized to obtain a desired multipole field of arbitrary purity, i.e., with small contributions from other multipoles.

As already mentioned, very significant advantages can be achieved by using combinations of permanent magnets, as sources of the field, and materials with high permeability (μ -metal), as conductors of the magnetic flux. With properly tailored μ -metal, it is possible to concentrate the magnetic field lines, and thereby increase the field magnitude. The largest field obtainable is the saturation induction, B_{sat} , of the material. From this point of view, the best material is the alloy iron-cobalt (≈ 50 – 50%), with $B_{\text{sat}} = 2.3$ T. For magnetic field values smaller than this, the permeability is always larger than 10^3 . Not only are these materials cheaper than REMs, they can be machined to tolerances of $10 \mu\text{m}$, a factor of ten higher than the tolerances achievable with REMs. One can therefore construct miniaturized configurations and experimentally realize magnetic multipoles with high purity. As a consequence of the high field intensities and the small dimensions achievable, it is possible to obtain

extremely large field gradients. This fact assumes a crucial importance in constructing atom traps for spectroscopy: the steeper the trap potential, the higher the motional averaging of the Zeeman broadening experienced by a trapped atom [11]. Moreover, steep traps are necessary in order to observe the quantum motion of trapped atoms [12]. In addition, a clear advantage of the combined system is that one can construct different μ -metal surrounds, which produce different magnetic fields, while using the same permanent magnets. The μ -metal-REM combination also simplifies the implementation of other trap requirements, like optical access to the trapping region. Finally, the use of combined configurations allows a simple adjustment of the REM operating point on the demagnetization curve.

In contrast to a system built only with permanent magnets, the inclusion of μ -metal severely complicates the calculation of the field. The calculation of a field, when the source is defined and the permeability is uniform, is always reducible to the evaluation of a straightforward integral. In such cases, it is possible to optimize the source distribution to achieve a particular potential and field configuration having high magnitude and purity (for example $2n$ -pole plane or spherical potential). On the other hand, when two media with different permeabilities (e.g., vacuum and μ -metal) are present, it is not possible to construct a simple solution, except in the most elementary cases. Usually these problems are solved by iterative, numerical methods and large computing facilities.

The method we discuss is a non-iterative finite-element algorithm that allows the calculation of the magnetic field from a cylindrically symmetric combination of permanent magnets and unsaturated μ -metal. The algorithm is based on Galerkin's method [13] and can be easily implemented on small-scale computers. In addition to magnetic problems, one can also apply the method to the evaluation of electric potentials (and consequently electric fields and capacitance matrices) in configurations where conductors and electric charges are present. As an example, we will refer to the design of a spherical quadrupole magnetic trap for neutral atoms.

1 Calculation of the field

In a current-free region of space it is always possible to define a potential φ such that the magnetic field \mathbf{H} is given by $\mathbf{H} = -\nabla\varphi$. If the magnetic potential is produced by a magnetization distribution $\mathbf{M}(\mathbf{x})$, one can define a "magnetic charge density" $\varrho \equiv -\nabla \cdot \mathbf{M}$. The potential φ is then calculated by integrating the Poisson equation. With these assumptions, the static Maxwell equations for the magnetic and the electric case are formally identical, and the determination of the magnetic field is completely equivalent to the determination of the electric field. For a homogeneous magnetization inside the magnets, the potential is given by the surface integral:

$$\varphi(\mathbf{r}) = \int_S \frac{\mathbf{M}(\mathbf{r}') \cdot d\mathbf{a}'}{|\mathbf{r} - \mathbf{r}'|} = \frac{B_r}{4\pi} \int_S \frac{\hat{\mathbf{n}}(\mathbf{r}') \cdot d\mathbf{a}'}{|\mathbf{r} - \mathbf{r}'|}. \quad (1)$$

In (1) B_r indicates the remanence of the material; the expression is valid if the permeability is uniform everywhere. Since the intrinsic permeability of a rare-earth magnet differs very little from that of vacuum ($1.04 \leq \mu_{\text{REM}} \leq 1.07$), (1) provides an accurate and straightforward way to calculate the magnetic field generated in free space by a REM distribution. The same would not hold for Alnico, for example, for which $\mu \approx 5$. If, in addition to REMs, the configuration contains materials with permeability $\mu \neq 1$, the magnetization induced by the magnets in this material has to be taken into account. As already mentioned, the calculation of the field is not, in such cases, a trivial task. However, if the permeability μ of a material is much larger than one, it can be shown that the surface interface between the vacuum and this material is an equipotential for φ [14]. Therefore, the problem of determining the magnetic field of a configuration of permanent magnets in the presence of μ -metal reduces to the determination of the electric field produced by a distribution of surface charges in the presence of conducting bodies. Because of the equivalence between the magnetic and the electric cases and because the electric case is more intuitive, we will treat the electrostatic problem.

If no conductors are present, the potential can be determined via (1). As an example, let us consider the distribution shown in Fig. 1a. The charge distribution is equivalent to two rings of permanent magnet (Fig. 1b), magnetized along the axis and with the north poles facing each other. We name this potential $V_0(\mathbf{x})$. Let us now introduce an arbitrary number M of electrically neutral conductors, isolated from one another. Figure 1c shows the conducting bodies added to the charge distribution of Fig. 1a. Note that the three conducting bodies have a hole along the axis. Because of the already existing electric field, there is a redistribution of the surface

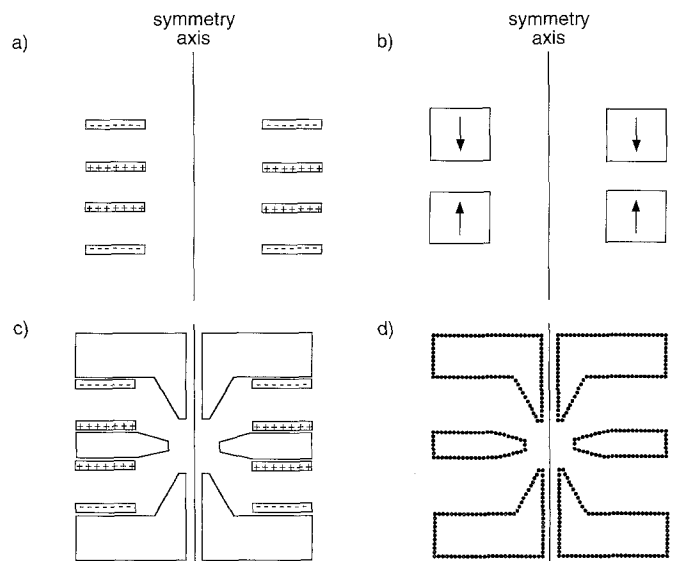


Fig. 1a-d. Sample model with cylindrical symmetry. Surface charges (a) equivalent to two rings of permanent magnets (b). The electric field resulting by the insertion of the conductors (c) can be evaluated by the partition (d)

charges on each conductor, such that the new electric potential $V(\mathbf{x})$ assumes a constant value on each conductor's surface. We define V_α as the potential and Q_α as the total charge on the α -th conductor. In the magnetic case we can set $Q_\alpha = 0$ because there is no magnetic monopole. We wish to calculate the new charge distribution on each conductor. Once this is known, it is possible to determine the potential, and consequently the field, everywhere.

We first partition the surface of the conductors into elements. The partition elements need not be contiguous. Elements belonging to the same conductor are assumed to be electrically connected. The dimensions of the elements are chosen such that the potential $V_0(\mathbf{x})$ remains constant on the surface of each of them to the calculational accuracy desired. Let N_α be the number of elements into which the α -th conductor is divided. The partition order N is then defined as

$$N \equiv \sum_{\alpha=1}^M N_\alpha.$$

A possible partition into rings of the sample conductors is illustrated in Fig. 1d. We name the potential, the charge and the value of the potential $V_0(\mathbf{x})$ at the i -th element ($i = 1 \dots N$) respectively v_i , q_i and v_{0i} . The presence of a charge on the i -th element induces a change $\Delta V_i(\mathbf{x})$ in the potential. The previous condition on the size must still hold for any potential contribution $\Delta V_i(\mathbf{x})$. We name this general requirement *condition 1*. From superposition, the change in the potential on the j -th element due to a charge q_i on the i -th element can be written as,

$$\Delta v_j \equiv \sum_{i=1}^N D_{ji} q_i. \quad (2)$$

In order to simplify the following argument, it is convenient to introduce a vectorial notation to describe the potential and the charge on the elements and the interactions between them. The potential and the charge on all the elements can be described by considering the N -dimensional vectors \mathbf{v} , \mathbf{v}_0 , $\Delta \mathbf{v}$ and \mathbf{q} (\mathbf{v} , \mathbf{v}_0 , $\Delta \mathbf{v}$, $\mathbf{q} \in \mathbb{R}^N$), whose i -th component gives respectively the potentials v_i , v_{0i} , Δv_i and the charge q_i on the i -th conducting element. The scalar product and common matrix operations are defined as usual. Equation (2) becomes $\Delta \mathbf{v} = \mathbf{D}\mathbf{q}$. The matrix \mathbf{D} is the inverse of the capacitance matrix \mathbf{C} of the system of N elements:

$$\mathbf{D} = \mathbf{C}^{-1}.$$

\mathbf{D} can be calculated from the shape of the elements. Completing the definitions, let \mathbf{w}_α be the vector such that:

$$(\mathbf{w}_\alpha)_i = \begin{cases} 1 & \text{if the } i\text{-th element belongs to the conductor } \alpha \\ 0 & \text{otherwise.} \end{cases}$$

The potential \mathbf{v} is now given by:

$$\mathbf{v} = \mathbf{v}_0 + \mathbf{D}\mathbf{q} = \mathbf{v}_0 + \mathbf{C}^{-1}\mathbf{q}. \quad (3)$$

The conditions that on every conductor α the potential must keep the same value V_α and that the whole

charge Q_α must be zero are now written:

$$\mathbf{v} = \mathbf{w}_\alpha V_\alpha, \quad (4)$$

$$Q_\alpha = \mathbf{w}_\alpha \mathbf{q} = 0, \quad (5)$$

where we assume a sum on the repeated index. By using (4), (3) becomes

$$\mathbf{q} = \mathbf{C}(\mathbf{v} - \mathbf{v}_0) = V_\alpha \mathbf{C}\mathbf{w}_\alpha - \mathbf{C}\mathbf{v}_0. \quad (6)$$

In the last expression the capacitance matrix \mathbf{C} appears, which is calculated by direct inversion of the matrix \mathbf{D} . Since both matrices have dimension N^2 and N is usually not a small number, the main effort in the calculation lies in the inversion operation of \mathbf{D} . By forming the product $\mathbf{w}_\beta \cdot \mathbf{q}$ in (6), and using (5), we have:

$$0 = Q_\beta = \mathbf{w}_\beta \mathbf{q} = V_\alpha \mathbf{w}_\beta \mathbf{C}\mathbf{w}_\alpha - \mathbf{w}_\beta \mathbf{C}\mathbf{v}_0, \quad (7)$$

and

$$\mathbf{w}_\beta \mathbf{C}\mathbf{w}_\alpha V_\alpha = \mathbf{w}_\beta \mathbf{C}\mathbf{v}_0, \quad 1 \leq \alpha, \beta \leq M. \quad (8)$$

The last relation is a system of equations in the variables V_α , whose order is equal to the number M of conductors. The $M \times M$ matrix \mathbf{K} formed by the elements $\mathbf{w}_\beta \mathbf{C}\mathbf{w}_\alpha$ is determined solely by the geometry of the conductor system. The system of equations can be easily solved by numerically inverting this matrix. By putting the V_α coefficients back into the (6), it is now possible to evaluate the amount of charge on every element, and consequently to calculate the potential, and then the field, everywhere.

Note that it is not difficult to recognize the matrix \mathbf{K} as the capacitance matrix of the system of the M conductors. In fact, assuming no charge distribution ($\mathbf{v}_0 = 0$) and that each conductor α has a charge Q_α , one gets an expression similar to (7):

$$Q_\beta = \mathbf{w}_\beta \mathbf{C}\mathbf{w}_\alpha V_\alpha.$$

The M -dimensional vector formed by the M values of $\mathbf{w}_\beta \mathbf{C}\mathbf{v}_0$ is again determined by the conductor geometry together with the details of the distribution of charges producing the field.

Like all other finite-element numerical methods, the choice of the partition (mesh) constitutes a crucial step of the procedure. We have already given condition 1 dictating the size of the partition elements. For a given partition order, this condition can be always satisfied if the dimensions of the elements are chosen small enough. However, there is a limit to the smallness of the elements. This can be shown by using the following argument. Assume an arbitrary surface to be described by a partition with small spheres, for example by replacing it with a layer of spheres having radius ε and reciprocal distances d_{ij} . In such a case, the matrix $\mathbf{D} = \mathbf{C}^{-1}$ is simply given by:

$$D_{ij} = \frac{1}{\varepsilon}, \quad \text{if } i=j;$$

$$D_{ij} = \frac{1}{d_{ij}}, \quad \text{if } i \neq j.$$

In order to satisfy condition 1, $\varepsilon \ll d_{ij}$, for every $i, j \neq i$. We can define \mathbf{D}' such that:

$$\mathbf{D} = \frac{1}{\varepsilon} \mathbf{I} + \mathbf{D}',$$

where \mathbf{I} is the identity matrix. Therefore, the matrix \mathbf{D}' has the diagonal elements equal to zero and the off-diagonal ones equal to those of \mathbf{C}^{-1} . It follows: $\mathbf{C}^{-1} = (1/\varepsilon) (\mathbf{I} + \varepsilon \mathbf{D}')$ and so $\mathbf{C} = \varepsilon (\mathbf{I} + \varepsilon \mathbf{D}')^{-1}$. If ε is such that for all eigenvalues λ' of \mathbf{D}' , $\varepsilon |\lambda'| \ll 1$, and one can write:

$$\mathbf{C} = \varepsilon [\mathbf{I} - \varepsilon \mathbf{D}' + \mathbf{O}(\varepsilon^2)],$$

where $\mathbf{O}(\varepsilon^2)$ is a matrix with eigenvalues of order ε^2 . Evaluating the capacitance of the conductor α :

$$\mathbf{w}_\alpha \mathbf{C} \mathbf{w}_\alpha \cong \varepsilon \cdot \mathbf{w}_\alpha (\mathbf{I} - \varepsilon \mathbf{D}') \mathbf{w}_\alpha = \varepsilon N_\alpha - \varepsilon^2 \mathbf{w}_\alpha \mathbf{D}' \mathbf{w}_\alpha.$$

Note the capacitance vanishes as the radius of the spheres becomes smaller and smaller. The physical reason for this behavior is clear: if $\varepsilon \rightarrow 0$, the mutual interaction D_{ij} between two spheres becomes negligible in comparison with the self-interaction D_{ii} of a single sphere. Generalizing, we have an additional condition on the partitioning of the configuration: the diagonal elements of the matrix \mathbf{C}^{-1} , describing the self-interaction, must have the same magnitude as the largest off-diagonal elements, which describe the mutual interaction. We call this *condition 2*.

The previous argument also shows that a finite set of spheres cannot provide a "good" partition. In fact, in the case of a partition with spheres, the condition 2 corresponds to $\varepsilon \approx d_{ij}$ (for some i and $j \neq i$). Such a relation does not agree with the condition 1, $\varepsilon \ll d_{ij}$ (for every i and $j \neq i$).

2 Cylindrically symmetric configurations

Let us restrict now the discussion to problems exhibiting a cylindrical symmetry. In this case, the most natural candidates for the elements are tori, whose axes are

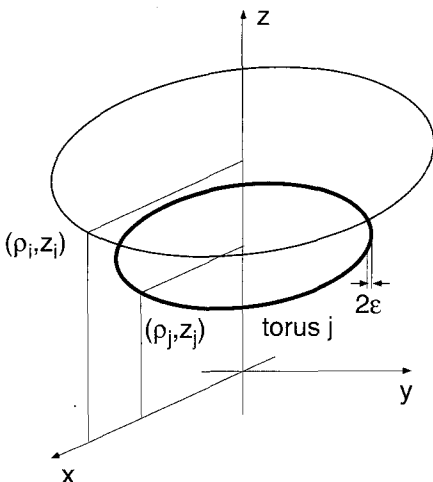


Fig. 2. Geometry of a partition in tori

coincident with the symmetry axis of the configuration (Fig. 2). This partition geometry is also illustrated in the sample configuration of Fig. 1. For each element j , the thickness 2ε must be much smaller than the torus radius ϱ_j . We assume a unity charge uniformly distributed over its surface. In this case, the potential generated by torus j at coordinates (ϱ_i, z_i) is:

$$V_j(\varrho_i, z_i) = \frac{2}{\pi s} E\left(\frac{4\varrho_i\varrho_j}{s^2}\right), \quad (9)$$

where

$$s = \sqrt{d^2 + 4\varrho_i\varrho_j}, \quad d = \sqrt{(\varrho_i - \varrho_j)^2 + (z_i - z_j)^2}.$$

ϱ_j and z_j are the cylindrical coordinates of the intersection of the torus j with the half-plane $\varphi = 0$. The function E is the elliptic integral^[15]:

$$E(m) = \int_0^{\frac{\pi}{2}} \frac{d\theta}{\sqrt{1 - m \sin^2 \theta}}.$$

On the surface of torus j , $d = \varepsilon$, and the potential (9) can easily be evaluated using the limiting form of $E(m)$: $\lim_{m \rightarrow 1} E(m) = \log(4/\sqrt{1-m})$. The result is:

$$V_j(\varrho_i, z_i \text{ on the surface}) \cong \frac{1}{\pi \varrho_j} \log \frac{8\varrho_j}{\varepsilon}. \quad (10)$$

Equations (9) and (10), respectively, give the off-diagonal and the diagonal terms of the matrix \mathbf{D} . Because of the logarithmic dependence, it is possible to choose the parameter ε and the partition order N in order to satisfy both condition 1 and condition 2 for the size and shape of the elements.

We first tested the method by calculating the capacitance of a sphere with unity radius ($C = 1$), by using a partition of rings. Figure 3 shows the results: the curves give the percent error $1 - C_{\text{calc}}/C$ for different values of the radius ε and for $N = 50, 100, 200$ and 400 . Note that the precision increases with the partition order and that

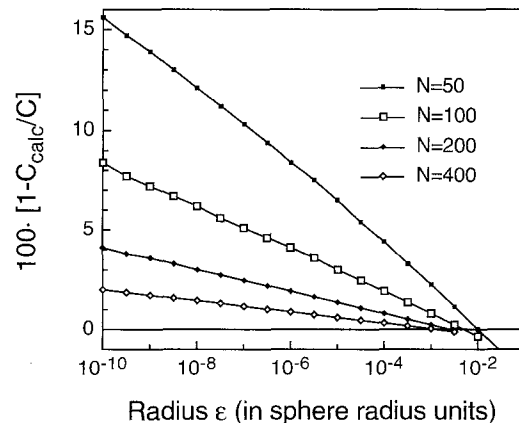


Fig. 3. Capacitance of a conducting sphere, calculated with torus partitions of different order N , as a function of the torus radius ε

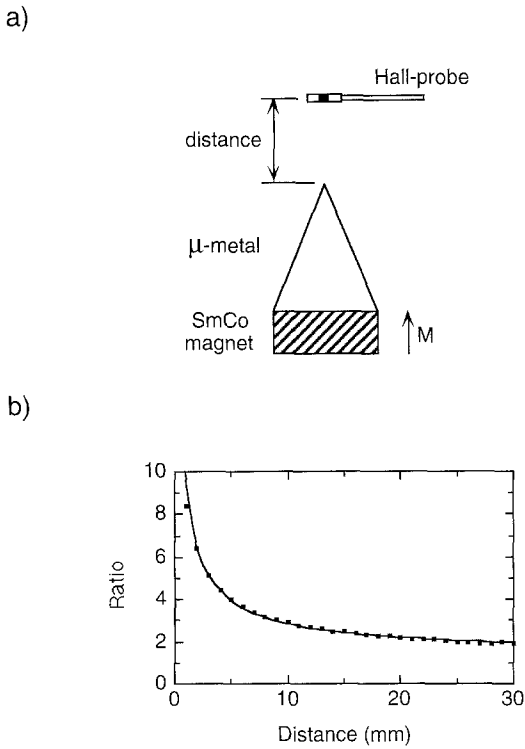


Fig. 4a, b. Test configuration (a). The curve in the graphic (b) represents the calculated ratio of the axial magnetic field with and without the iron cone. The dots show the measured values

the result has only a mild logarithmic dependence on ϵ . In analogy to the partition with spheres discussed previously, the precision becomes worse if $\epsilon \rightarrow 0$. For this and all other calculations we have used a workstation (Personal Iris, Silicon Graphics Inc.).

We have also tested the method for the case described in Fig. 4a. For such a configuration, a simple analytical calculation of the magnetic field does not exist. The calculated quantity is the ratio between the axial component of the magnetic field with and without the μ -metal cone (iron). The partition order N used in the calculation is 400. The same quantity was also measured with a Hall probe. The measured and calculated values are compared in Fig. 4b. The agreement between calculation and measurements is evident.

3 Design and test of a magnetic trap

We used the method to calculate the magnetic field for the configuration of Fig. 1c. This electric configuration is equivalent to the magnetic quadrupole trap shown in Fig. 5. The field magnitude on the $\rho-z$ plane is shown with a grey scale in Fig. 6. The diameter of the trapping region is 15 mm. The magnetic flux is generated by eight permanent magnets (samarium-cobalt, $B_r = 1 \pm 0.05$ T) and is guided into the configuration center with a μ -metal surround (iron-cobalt). In the trapping region, the field has a quadrupole structure. The trap has eight apertures into the center. Furthermore, both μ -metal endcaps have

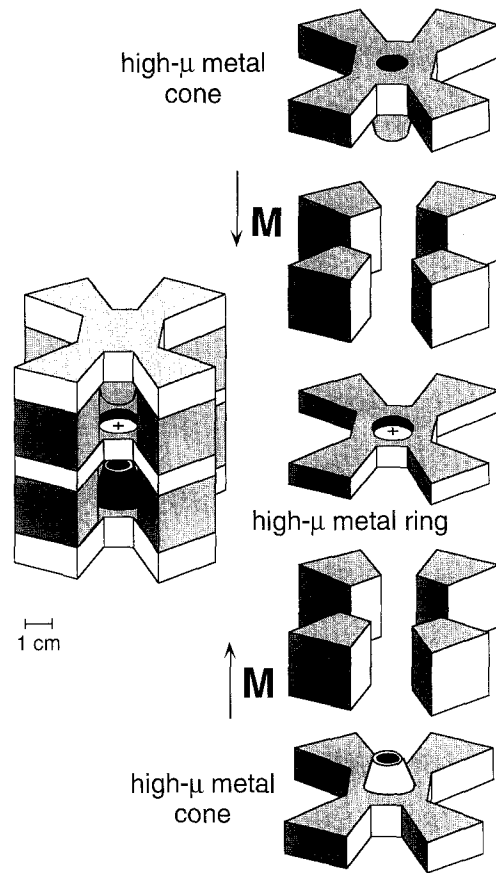


Fig. 5. Explosion representation of the trap. The small cross indicates the center of the trap ($\rho=0, z=0$). The z -axis is vertical

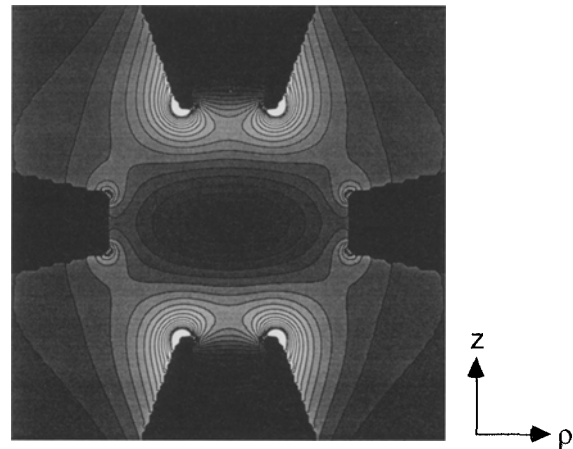


Fig. 6. Magnetic field magnitude in the central region of the trap. The field difference between two adjacent lines (representing surfaces with equal field intensity) is 40 mT. The center of the picture corresponds to the center of the trap ($\rho=0, z=0$).

5 mm diameter cylindrical holes, allowing access along the symmetry axis.

The magnetic materials near the center of the trap are cylindrically symmetric, and therefore the dominant contribution to the trapping field is also cylindrically symmetric. The outer bulk of the trap is clearly not cylindrically symmetric, but it is far from the trapping region; its influence is therefore weak enough that we can assume

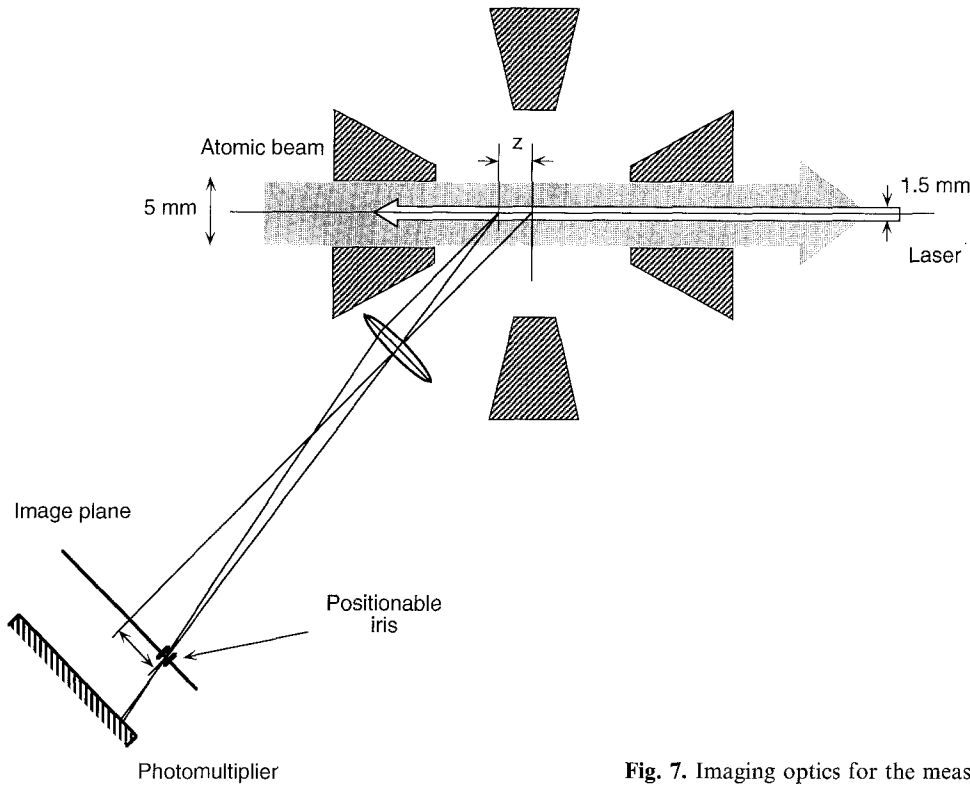


Fig. 7. Imaging optics for the measurement of the field gradient and shape

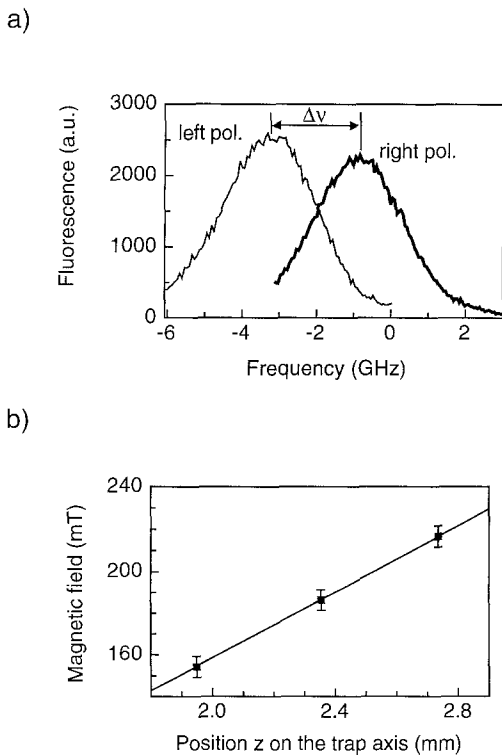


Fig. 8a, b. Fluorescence spectra (a) from a point on the trap axis for both circular polarizations of the excitation laser. The laser frequency is given relative to the D_2 transition frequency of ${}^7\text{Li}$. The dependence of the measured magnetic field on the position of the trap axis point is shown in (b)

cylindrical symmetry for purposes of calculation. The magnets fill only half the possible volume of two complete rings; we compensated by halving the remanence. Moreover, the self-capacitance of the partition rings corresponding to the external part of the bulk was also reduced by a factor of two. The calculated value of the z -component of the field gradient on the axis is: 0.81 ± 0.04 T/cm. The error is due to the uncertainty in the remanence of the material. The axial gradient is constant within 2% inside a length of 8 mm on the axis, which corresponds to a quadrupole field of high purity. A second version of the trap was also constructed, without the two axial holes and with a smaller trapping region. The calculated value of the gradient for this configuration is 5 T/cm.

The shape and the gradient of the magnetic field were then determined spectroscopically. An atomic beam of lithium was sent through the trap along the z -axis. The atomic beam was illuminated with a laser beam (beam waist 1 mm) carefully aligned along the same axis. The laser beam was generated by a 671 nm laser diode, grating stabilized at a linewidth of 2 MHz [16]. The laser light was tuned to the D_2 resonance of lithium. With imaging optics (Fig. 7) the fluorescence of the atoms was measured at successive points on the axis. The atoms are excited in the Paschen-Back regime. Figure 8a shows two spectra, obtained with σ^+ and σ^- polarized light, respectively. The spectra are broadened due to the Doppler effect, the hyperfine structure of the lines, and the finite size of the laser beam. The frequency of the spectra's maxima was determined by fitting a parabola to each

maximum and minimizing χ^2 . The difference Δv between the two frequencies depends only on the magnetic field at the imaged axial point. Measuring the Zeeman splitting at different points and knowing the magnification of the imaging optics, it is possible to determine the value of the field gradient. Figure 8b shows the measured fields at three points. The fact that the points lie precisely on a straight line, corresponds to a constant gradient and thus to a quadrupole field. The calculated value for the gradient is 0.71 ± 0.04 T/cm. The assigned error takes into account the uncertainty in the alignment of both the atomic and laser beams and in the determination of the imaging magnification. The 12% deviation from the calculated value is mainly caused by the flux losses in the eight apertures. These apertures break the external cylindrical symmetry of the trap, an effect that is very difficult to calculate. Moreover, the fact that the REM permeability is slightly larger than one ($1.04 \leq \mu \leq 1.07$), can also cause a reduction of the field coupled into the trapping region. The results are however in good agreement with the calculations. In addition, the method was also employed to design a successful Penning trap.

4 Conclusion

In summary, we have theoretically described a method that allows the calculation of magnetic (electric) fields produced by permanent magnets (charges) and in the presence of highly permeable materials (conductors). We have discussed in detail the case of cylindrically symmetric configurations. The method can be easily implemented on a small scale computer and provides results that are in very good agreement with experimental measurements. As an example we have reported the design of a magnetic trap for neutral atoms, for which the magnetic

field shape and gradient were also determined experimentally.

Acknowledgements. We appreciate useful discussions with S. Ross and J. Walz. One of the authors (L.R.) is grateful to H. Klagges for the kind assistance in programming. This work was partially supported by the Deutsche Forschungsgemeinschaft under contract N° Ha 1457/4-1.

References

1. K. Halbach: Nucl. Instrum. Methods **169**, 1 (1980)
2. H.A. Leupold, E. Potenziani II: IEEE Trans. MD-**23**, 3628 (1987)
3. W. Gudat, J. Pflüger, J. Chatzipetros, W. Peatman: Nucl. Instrum. Methods A **246**, 50 (1986)
4. K. Halbach: Nucl. Instrum. Methods **187**, 109 (1981)
5. XU Qing: Nucl. Instrum. Methods A **253**, 173 (1987)
6. L.S. Brown, G. Gabrielse: Rev. Mod. Phys. **58**, 233 (1986)
7. A.L. Migdall, J.V. Prodan, W.D. Phillips, T.H. Bergeman, J. Metcalf: Phys. Rev. Lett. **54**, 2596 (1985)
8. H.F. Hess, G.P. Kochanski, J.M. Doyle, N. Masuhara, D. Kleppner, T.J. Greytak: Phys. Rev. Lett. **59**, 672 (1987)
9. R. van Roijen, J.J. Berkout, S. Jaakkola, J.T.M. Walraven: Phys. Rev. Lett. **61**, 931 (1988)
10. V. Frerichs, W. Kaenders, D. Meschede: Appl. Phys. A **55**, 242 (1992)
11. D. Kleppner: In *The Hydrogen Atom*, ed. by G.F. Bassani, M. Inguscio, T.W. Hänsch (Springer, Berlin, Heidelberg 1989) p. 109
12. T.H. Bergeman, P. McNicholl, J. Kycia, H. Metcalf, N.L. Balazs: J. Opt. Soc. Am. B **6**, 2249 (1989)
13. P.P. Silvester, R.L. Ferrari: *Finite Elements for Electrical Engineers*, 2nd edn. (Cambridge Univ. Press, Cambridge 1990) pp. 146-147
14. J.D. Jackson: *Classical Electrodynamics*, 2nd edn. (Wiley, New York 1975) pp. 190-191
15. M. Abramowitz, I.A. Stegun (eds.): *Handbook of Mathematical Functions* (Dover, New York 1965)
16. L. Ricci, A. Hemmerich, T. Esslinger, W. König, T.W. Hänsch: Opt. Commun. (submitted)